

1 Supporting Information

2

3

4 **Omnidirectional Diffusion of Organic Amine Salts Assisted by Ordered Arrays in Porous Lead**

5 **Iodide for Two-Step Deposited Large-Area Perovskite Solar Cells**

6

7 Jiacheng He, Wangping Sheng, Jia Yang, Yang Zhong, Yang Su, Licheng Tan^{*ac}, Yiwang Chen^{*abc}

8

9 Author contributions. J. H. and W. S. contributed equally to this work.

10 J. He, W. Sheng, J. Yang, Y. Zhong, Y. Su, Prof. L. Tan, Prof. Y. Chen

11 ^aCollege of Chemistry and Chemical Engineering/Institute of Polymers and Energy Chemistry (IPEC),

12 Nanchang University, 999 Xuefu Avenue, Nanchang 330031, China

13 Prof. Y. Chen

14 ^bNational Engineering Research Center for Carbohydrate Synthesis/Key Lab of Fluorine and Silicon

15 for Energy Materials and Chemistry of Ministry of Education, Jiangxi Normal University, 99 Ziyang

16 Avenue, Nanchang 330022, China

17 Prof. L. Tan, Prof. Y. Chen

18 ^cPeking University Yangtze Delta Institute of Optoelectronics, Nantong 226010, China

19 E-mail: ywchen@ncu.edu.cn (Y. C.); tanlicheng@ncu.edu.cn (L. T.)

20

21 **Experimental Section**

22 **Materials and Sample Preparation:** Unless specified, all chemicals are employed as received

23 without further modifications after purchase. Tin(IV) oxide (SnO₂, 15% in H₂O colloidal dispersion

24 liquid), isopropanol (99.7% purity) and lead iodide (PbI₂, 99.999%) were purchased from Alfa Aesar.

25 N,N-dimethylformamide (DMF, 99.8%), dimethyl sulfoxide (DMSO, anhydrous, ≥99.9%),

26 chlorobenzene (CB, 99.8%), acetonitrile (99.8%), 4-tert-butyl pyridine (tBP),

27 bis(trifluoromethane)sulfonimide lithium salt (Li-TSFI, 99.95%) were purchased from Sigma-Aldrich.

28 Formamidinium iodide (FAI, 99.8%), methylamine iodide (MAI, 99.5%), methylamine hydrochloride

29 (MAHI, 99.5%) were purchased from Xi'an Polymer Light Technology Corp. 2,2',7,7'-tetrakis(N,N-di-

30 p-methoxyphenylamine)-9,9-spirobifluorene (Spiro-OMeTAD, 99.5%) was purchased from

31 Luminescence Technology Corp. Succinamide (SA, >98%) was purchased from

32 TCI(Shanghai)Development Co., Ltd.

33

34 **Perovskite Precursor Preparation:** PbI_2 (691.5 mg, 1.5 mmol/mL) was dissolved in DMF/DMSO
35 (95:5) and stirred at 60 °C for 6 h for the pristine PbI_2 precursor solutions. For the SA- PbI_2 precursor
36 solutions, 5 mg succinamide was dissolved into 1 ml DMSO solutions, then PbI_2 (691.5 mg, 1.5
37 mmol/mL) was dissolved in DMF/DMSO with succinamide (95:5) and stirred at 60 °C for 6 h for the
38 SA- PbI_2 precursor solutions. The organic amine salts solution, FAI, MAI, MACI were dissolved in 2-
39 propanol with a concentration of 90, 6.4, and 9 mg mL⁻¹, respectively. The Spiro-OMeTAD solution
40 was prepared with a concentration of 72.3 mg mL⁻¹ in chlorobenzene, in which 28.8 μL of 4-tert-
41 butylpyridine and 17.5 μL of lithium (trifluoromethylsulfonyl)-imide (520 mg mL⁻¹ in acetonitrile)
42 were added as additives. It should be noted that both the PbI_2 and organic amine salt solutions need
43 to be fresh.

44

45 **PVSCs Fabrication and Characterization:** First, the indium tin oxide (ITO) glasses were cleaned by
46 sequentially washing with detergent, deionized (DI) water, acetone and isopropanol (IPA) for 20 min
47 then dried with a nitrogen (N_2) stream followed by air plasma treatment for 5 min before use. The
48 uniform and dense SnO_2 layer was deposited onto an ITO substrate by spin-coating SnO_2
49 nanoparticle solution (Alfa Aesar, tin(IV) oxide, 15% in H_2O colloidal dispersion, SnO_2 colloidal
50 solution/DI water, a ratio of 1:3) at 3000 rpm for 30 s, and annealed in ambient air at 150 °C for 30
51 min. Then treated in a plasma cleaning machine for 6 min. After that, 62 μL of the PbI_2 and SA- PbI_2
52 precursor solutions were spin-coated onto SnO_2 at 1500 r.p.m. for 30 s, then annealed at 70 °C for
53 1 min, and then cooled to room temperature. For the imprinted with SA, after SA- PbI_2 precursor
54 solutions were spin-coated onto SnO_2 at 1500 r.p.m. for 30 s, a silicon cylinder array stamp is placed
55 on the PbI_2 with moderated pressure (3 MPa) applying on it and heat treatment 70 °C for 1 min, the
56 silicon cylinder array stamp was removed. Subsequently, 75 μL of the (FAI/MAI/MACI) organic amine
57 salt solution was spin-coated on the top of the PbI_2 layer at 2000 rpm for 30 s, followed by thermal
58 annealing at 150 °C for 15 min. After the films were cooled down to room temperature, spiro-
59 OMeTAD solution was spin-coated on perovskite films at 4000 rpm for 30 s. Finally, a 100 nm Ag
60 anode was deposited by thermal evaporation (rate of 1.0 Å s⁻¹) using a metal shadow mask. The
61 device area was 0.04 cm². All devices' measurements were carried out in drying cabinet at room
62 temperature.

63

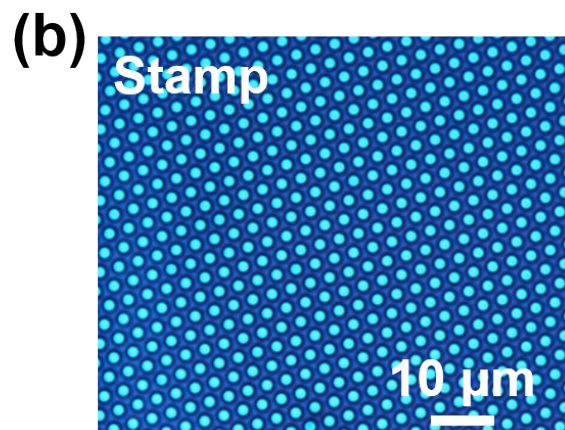
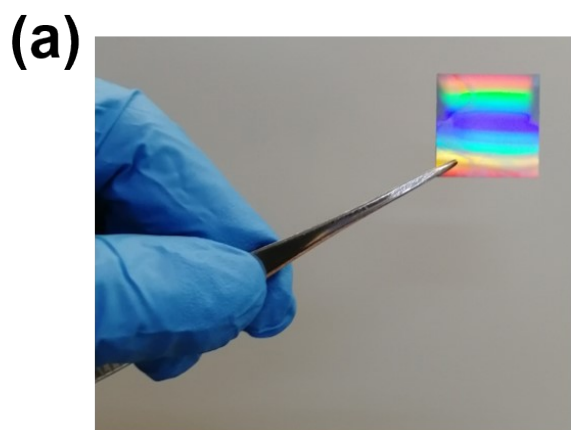
64 **Fabrication of perovskite solar module:**All layers except the spiro-OMeTAD and metal electrodes
65 were prepared in a low humidity air environment (<10% RH). Glass/ITO were ultrasonically cleaned
66 with acetone, deionized water, and isopropyl alcohol for 20 min, and then blown dry by nitrogen
67 (N₂) and treated with air plasma for 10 min. Then, a ~20 nm SnO₂ film was fabricated by meniscus-
68 printing (the blading speed is 10 mm/s and the distance between meniscus and substrate is 50 μm).
69 And the heating temperature was 50 °C. After that, the SnO₂ coated substrates were annealed at
70 150 °C for 30 min in air. A certain amount of SA-PbI₂ precursor solution (generally 75 μL for 5×5 cm²
71 substrate) was dripped into the gap (about 0.15 mm) between the blade coater and substrate, the
72 horizontal movement of blade coater was controlled by the computer with the speed of 15 mm/s.
73 A silicon cylinder array stamp was placed on the PbI₂ with moderated pressure (3 MPa) applying on
74 it and heat treatment 70 °C for 1 min, the silicon cylinder array stamp was removed. After the
75 substrate cooled down to room temperature, the mixture solution of FAI: MAI: MACl (90 mg: 6.4
76 mg: 9 mg in 1 mL IPA) was bladed onto the PbI₂ films (generally 100 μL for 5×5 cm²), then annealed
77 at 150 °C for 15 min for perovskite crystallization. The spiro-OMeTAD/CB solution (72.3 mg/mL) is
78 prepared by adding 28.8 μL 4-tertbutylpyridine, 17.5 μL Li-TFSI/acetonitrile solution (520 mg/mL).
79 The gap between blade and substrate is fixed at 50-100 μm and the blading speed is fixed at 5 mm/s.
80 Finally, about 100 nm of silver is deposited on the top of films by inkjet printing (DMP-2831-
81 Fujifilm).The solar module consisted of 6 sub-cells and the size of a single cell is 2.93 cm² (0.45 cm ×
82 6.5 cm), respectively.

83

84 **Device Characterizations:** Current density-voltage (*J-V*) characteristics were measured using a
85 source meter (Keithley 2400), equipped with a light source (100 mW/cm²) under AM 1.5 G
86 irradiation (Abet5 Solar Simulator Sun2000). The standard silicon solar cell was corrected from NREL
87 and the currents were detected under the solar simulator (Enli Tech, 100 mW cm⁻², AM 1.5 G
88 irradiation). The forward scan range is from 0 V to 1.2 V and the reverse scan range is from 1.2 V to
89 0 V and the scan rate for the *J-V* measurement is 0.2 V/s. The ¹H nuclear magnetic resonance (¹H-
90 NMR) spectrum was conducted by BRUKER/AVANCE NEO 300. The Ultraviolet-visible (UV-Vis)
91 spectra were characterized on UV-2600 spectrophotometer (Agilent Technologies Inc. Cary 5000
92 spectrophotometer). The steady-state photoluminescence (PL) spectra was recorded by

93 fluorescence spectrophotometer (Hitachi F-7000) and time-resolved photoluminescence (TRPL)
94 spectra were measured by fluorescence lifetime system (Light-Stone Instruments NTAS-TCSPC). FTIR
95 spectra were recorded on a Shimadzu IRPrestige-21 spectrometer. X-ray photoelectron
96 spectroscopy (XPS) measurement was performed in an ESCALAB 250Xi, Thermo Fisher (by using Al
97 $K\alpha$ X-ray source) under high vacuum (10^{-9} mbar) and the energy resolution was 450 meV. The
98 samples were coated on the highly conductive ITO substrates. Scanning electron microscopy (SEM)
99 was been conducted on SU8020 scanning electron microscope operated at an acceleration voltage
100 of 5 kV. Atomic force microscopy (AFM) images have been obtained by MultiMode 8- HR (Bruker)
101 atomic force microscope. X-ray diffraction (XRD) patterns were been performed by using Bruker
102 D8Discover 25 X-ray diffractometer. Electrical impedance spectroscopy (EIS) of the devices has been
103 performed in a frequency range from 1 MHz to 10 MHz using Zahner electrochemical workstation.
104 Dark J - V characteristics of the devices were tested at room temperature or within a cryostat
105 (HCS621G, Instec) by using a B1500A semiconductor analyzer (Keysight). The trap density of state
106 (tDOS) was performed using Agilent 4294A. The water contact angle has been recorded at a Krüss
107 DSA100s drop shape analyzer. External quantum efficiency (EQE) values were measured under
108 monochromatic illumination (Oriel Cornerstone 260 1/4 m monochromator equipped with an Oriel
109 70613NS QTH lamp), and the calibration of the incident light was performed using a monocrystalline
110 silicon diode.

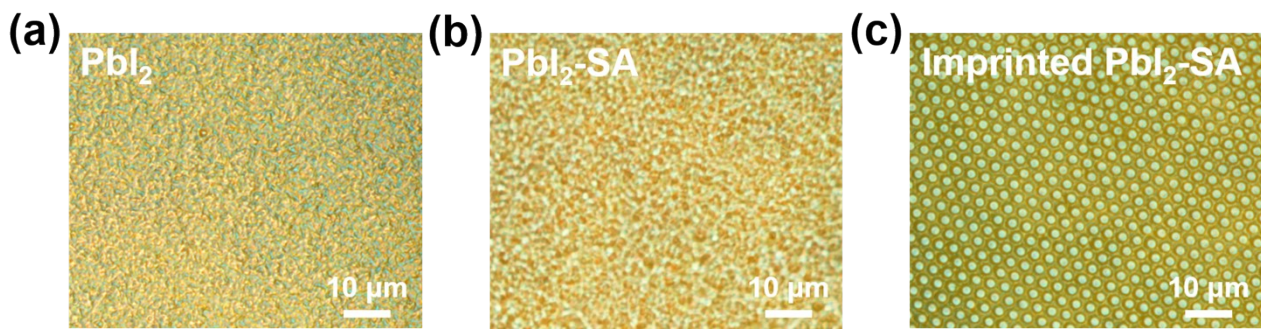
111



112

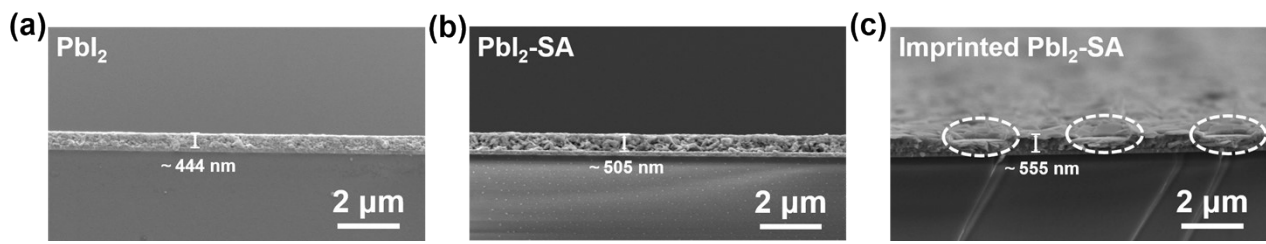
113 **Figure S1.** (a) Digital camera image of the silicon cylinder arrays stamp. It shows the visual effect of
114 optical interference owing to the diffraction-grating structure. (b) Optical microscope image of
115 silicon cylinder arrays stamp.

116

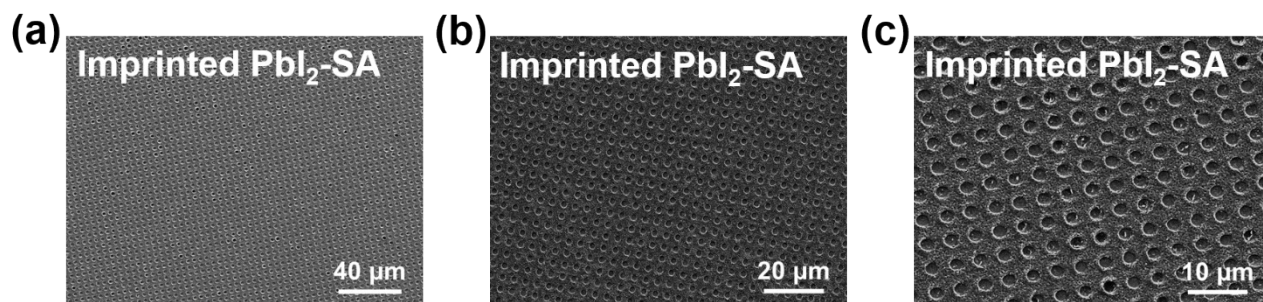


117
118 **Figure S2.** Optical microscope images of (a) Pbl₂, (b) Pbl₂-SA and (c) imprinted Pbl₂-SA films.

119



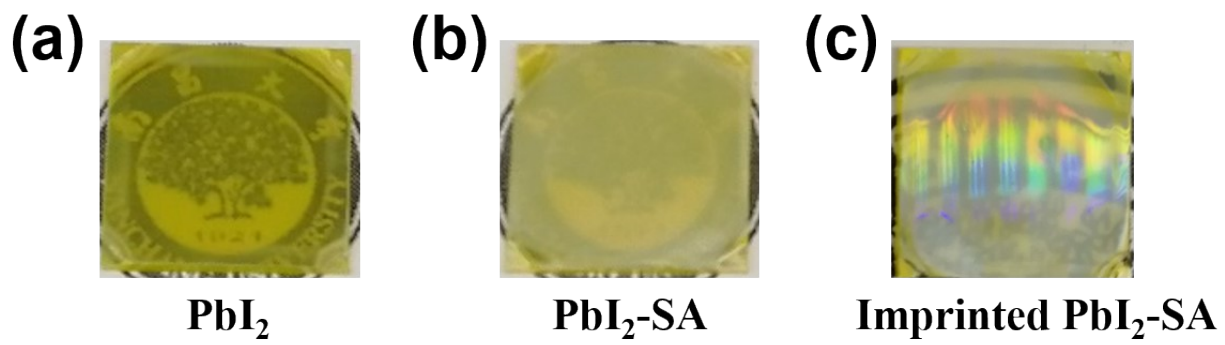
120
121 **Figure S3.** Cross-section SEM images of (a) Pbl₂, (b) Pbl₂-SA and (c) imprinted Pbl₂-SA films.
122



123

124 **Figure S4.** Top-view SEM images of imprinted Pbl₂-SA films at different magnifications to verify
125 uniformity.

126

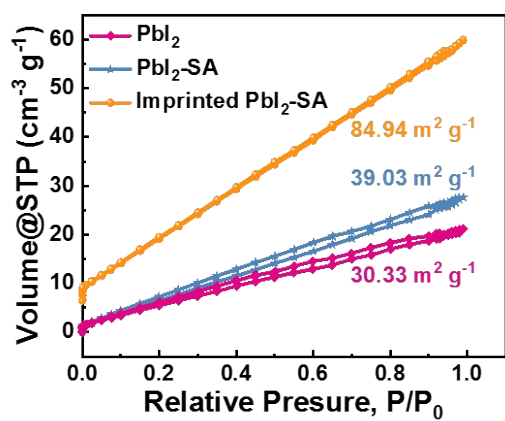


127

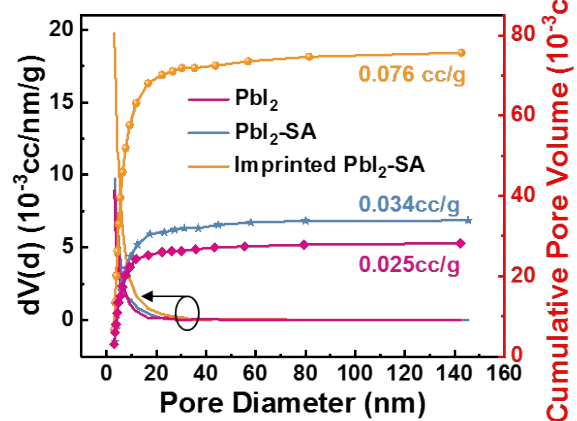
128 **Figure S5.** Photographs of (a) PbI₂, (b) PbI₂-SA and (c) imprinted PbI₂-SA films.

129

(a)



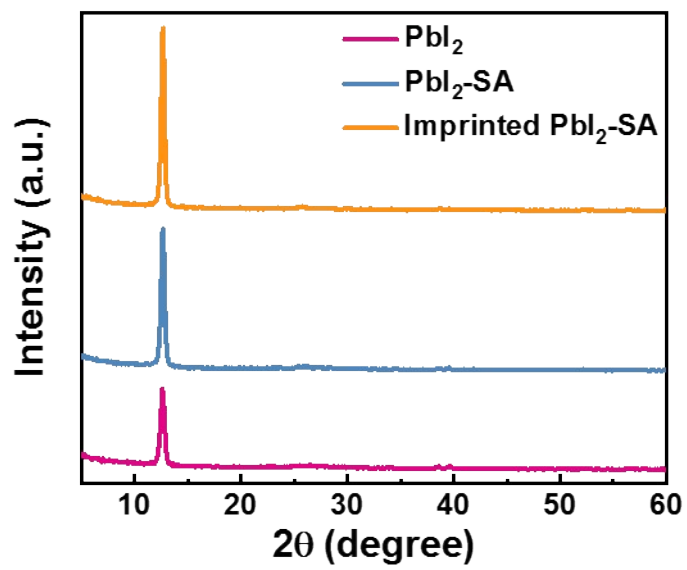
(b)



130

131 **Figure S6.** (a) Nitrogen adsorption and desorption isotherms, and (b) corresponding pore size
132 distribution for Pbl₂, Pbl₂-SA and imprinted Pbl₂-SA films.

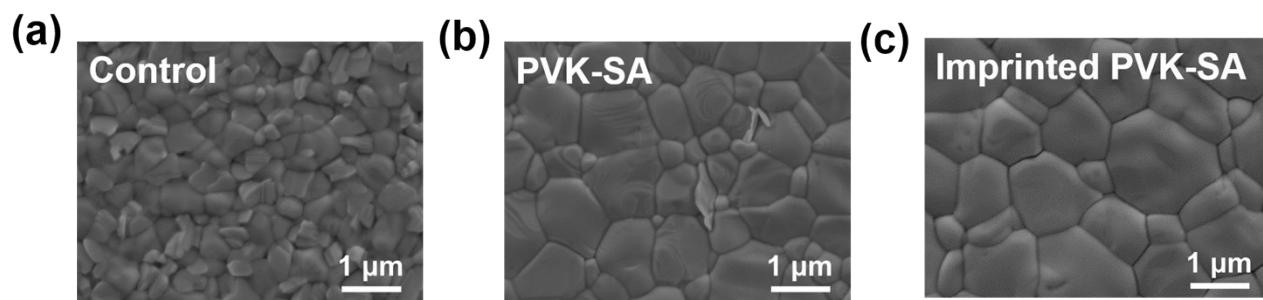
133



134

135 **Figure S7.** XRD patterns of Pbl₂, Pbl₂-SA and imprinted Pbl₂-SA films.

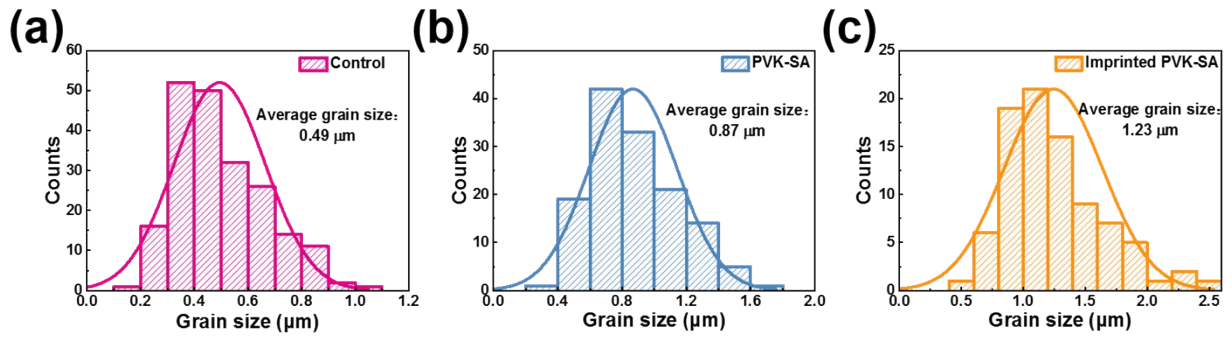
136



137

138 **Figure S8.** Top view SEM images of control, PVK-SA and imprinted PVK-SA perovskite films.

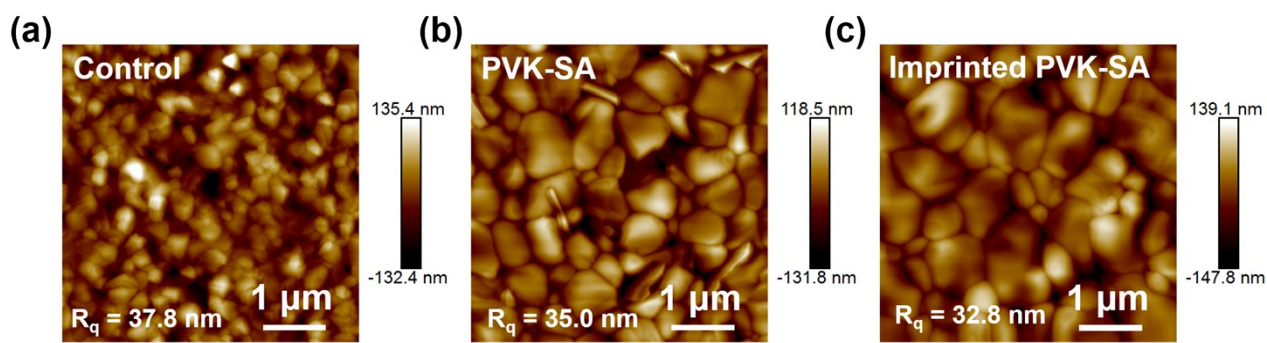
139



140

141 **Figure S9.** Grain size distributions extracted from SEM images of control, PVK-SA and imprinted PVK-

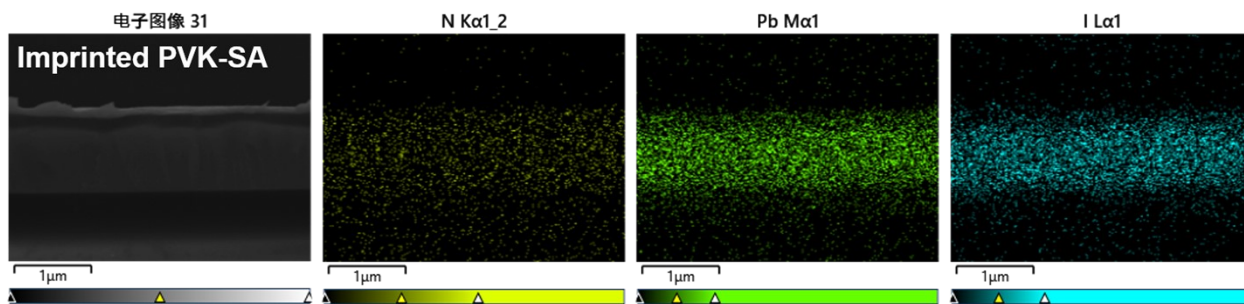
142 SA perovskite films.



143

144 **Figure S10.** AFM images of control, PVK-SA and imprinted PVK-SA perovskite films.

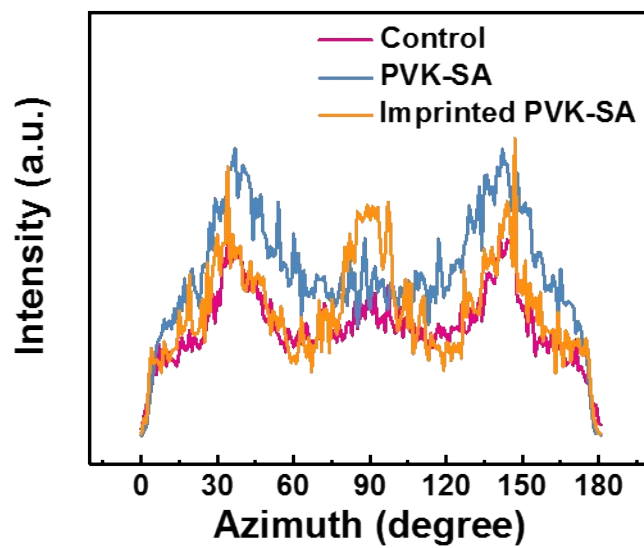
145



146

147 **Figure S11.** EDS mapping images of the imprinted PVK-SA perovskite film.

148

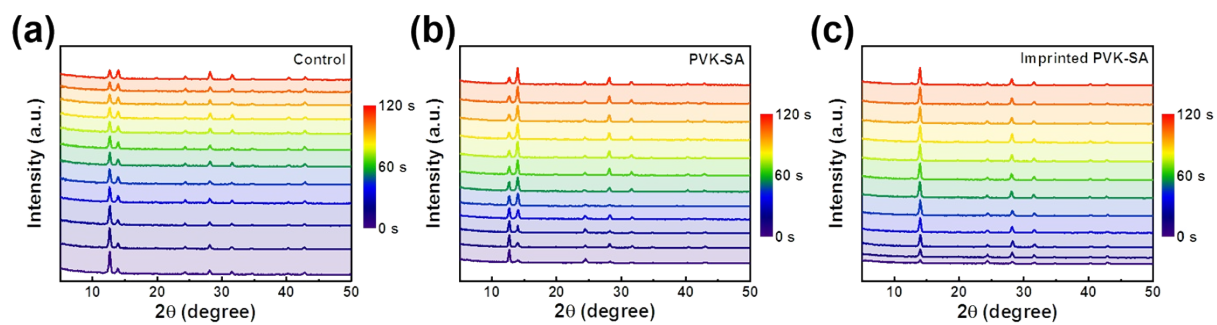


150

151 **Figure S12.** Radially integrated intensity plots along the ring at $q = 1.0 \text{ \AA}^{-1}$.

152

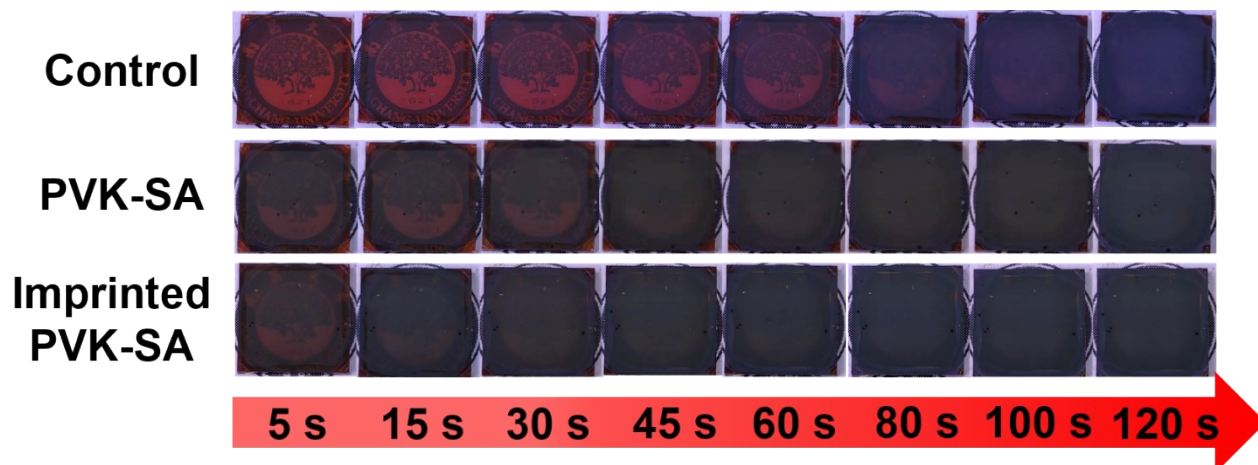
153



154

155 **Figure S13.** The semi-in situ XRD patterns of control, PVK-SA and imprinted PVK-SA perovskite films
156 annealing at 150 °C on the ITO/glass substrate.

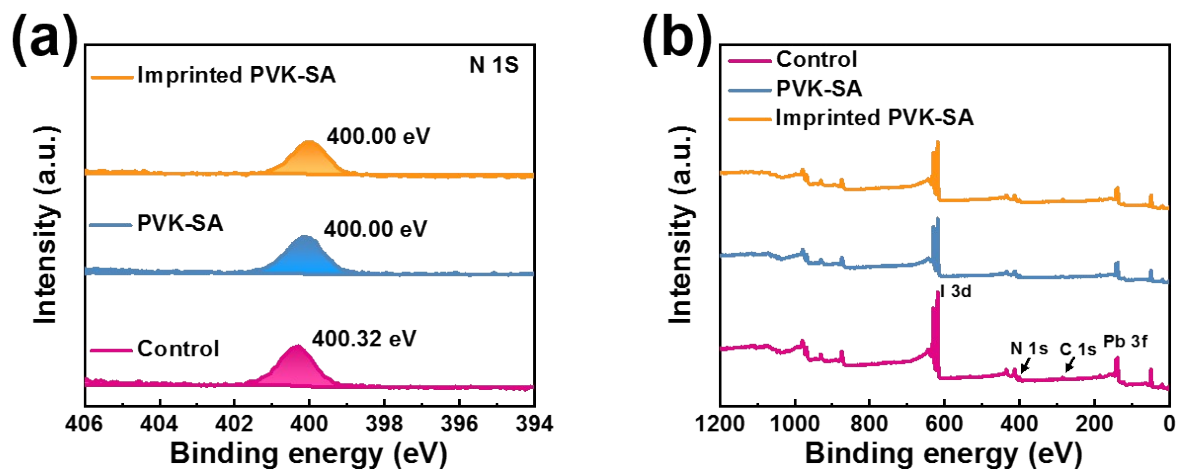
157



158

159 **Figure S14.** In-situ images of the control, PVK-SA and imprinted PVK-SA perovskite samples stored
160 in an ambient air (20% RH at 25 °C) for 120 s.

161

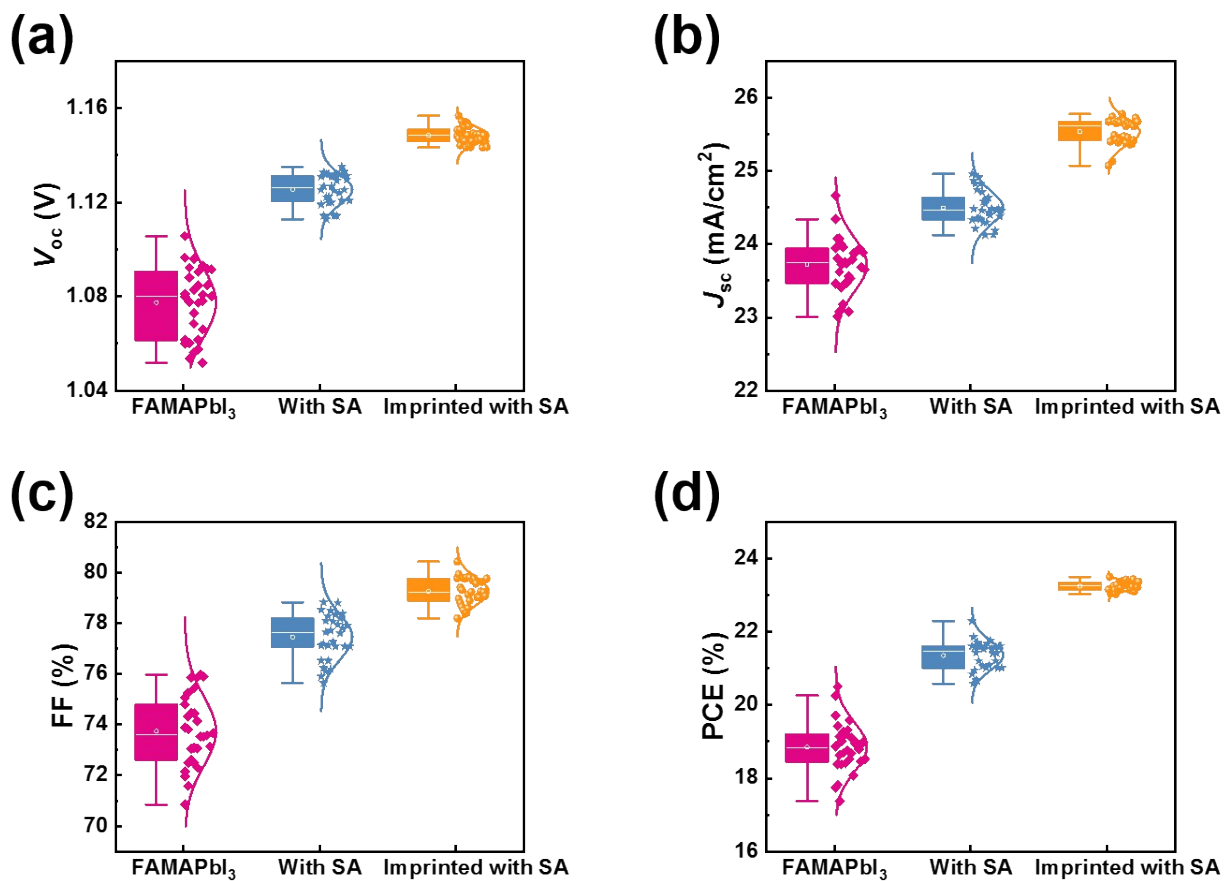


162

163 **Figure S15.** (a) XPS spectra N 1s in control, PVK-SA and imprinted PVK-SA perovskite films. (b) The

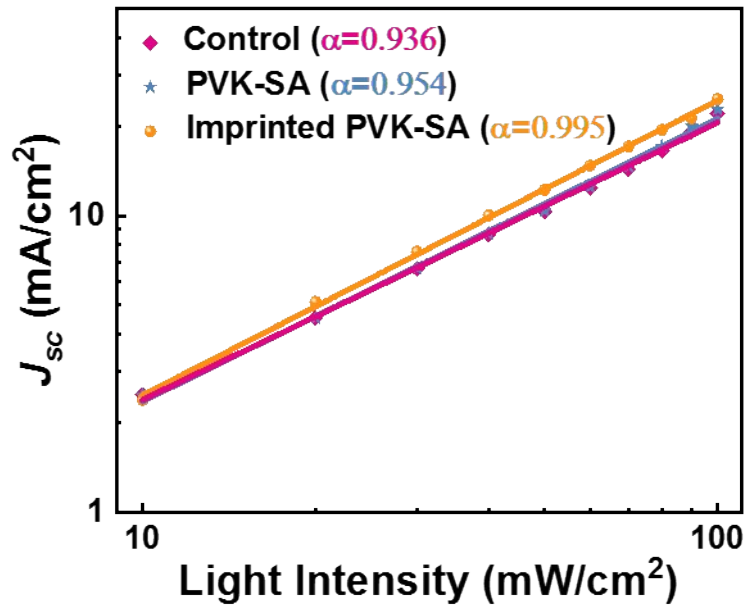
164 full XPS spectra of the perovskite films treatment in the range of 0 to 1200 eV binding energy.

165



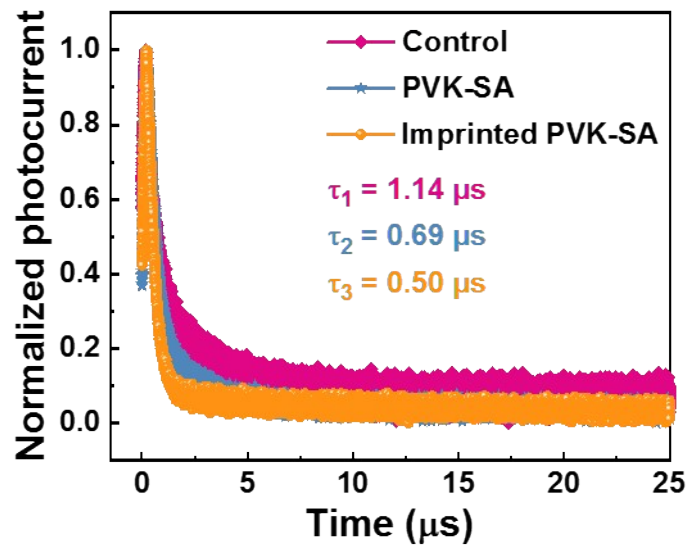
166

167 **Figure S16.** The statistical distribution of optoelectronic performance of control, PVK-SA and
 168 imprinted PVK-SA perovskite devices, respectively. (a) Open circuit voltage. (b) Short-circuit current.
 169 (c) Fill factor. (e) Power conversion efficiency.



170

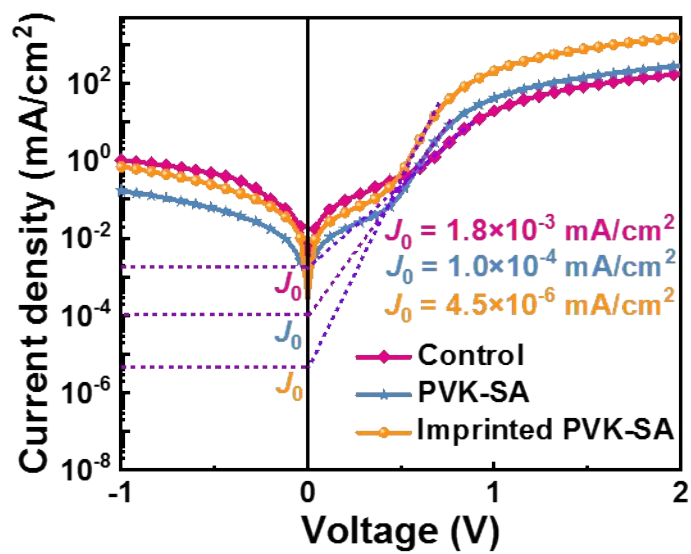
171 **Figure S17.** J_{sc} at various illumination intensities.



172

173 **Figure S18.** Transient photocurrent decay curves for control, PVK-SA and imprinted PVK-SA
174 perovskite devices, respectively.

175

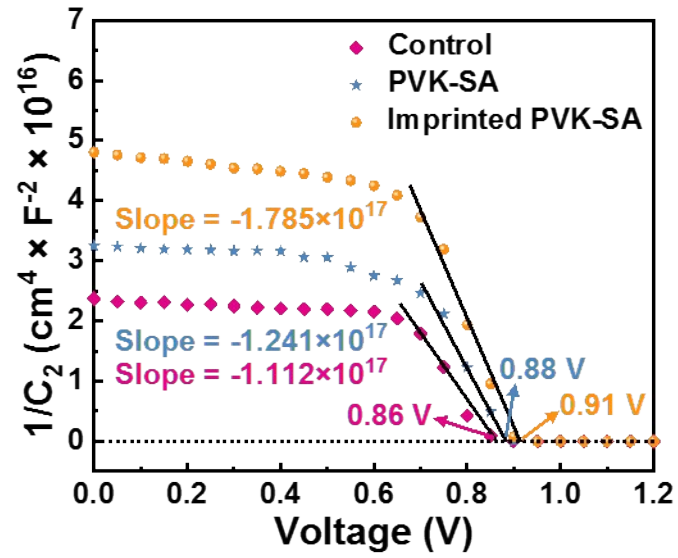


176

177 **Figure S19.** The dark current density-voltage (*J*-*V*) measurement of control, PVK-SA and imprinted

178 PVK-SA perovskite devices.

179



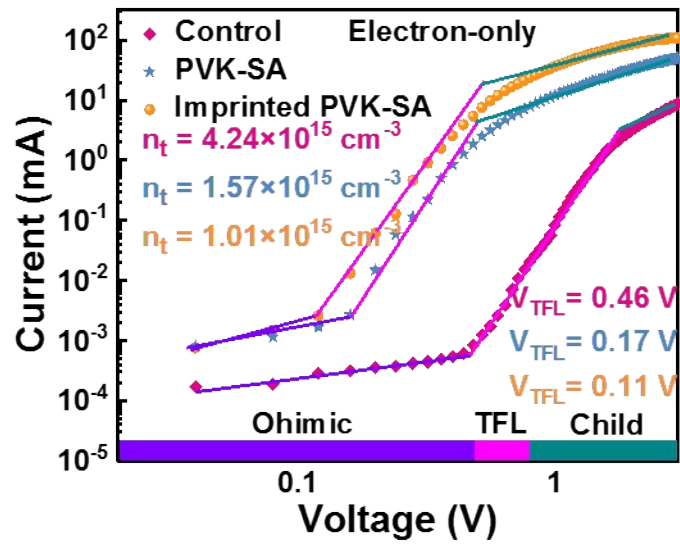
180

181 **Figure S20.** $1/C^2$ versus applied voltage plots (Mott-Schottky) in the control, PVK-SA and imprinted

182 PVK-SA perovskite devices.

183

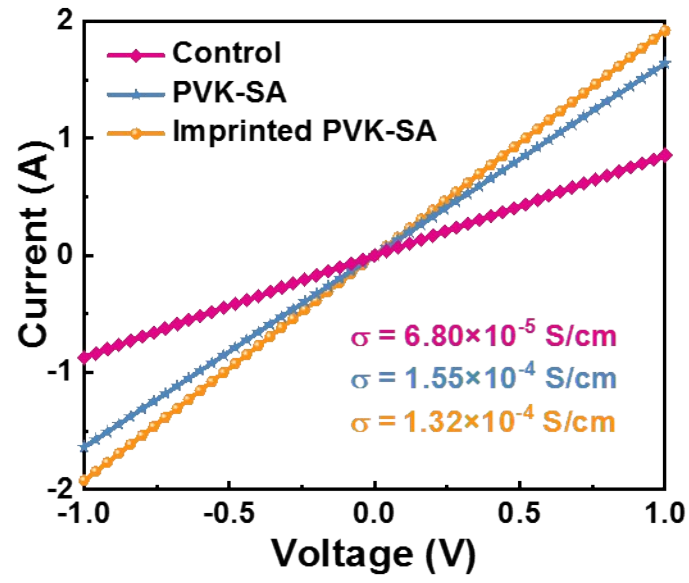
184



186

187 **Figure S21.** Space charge-limited current (SCLC) measurement of electron-only devices based on
 188 control, PVK-SA and imprinted PVK-SA perovskite devices.

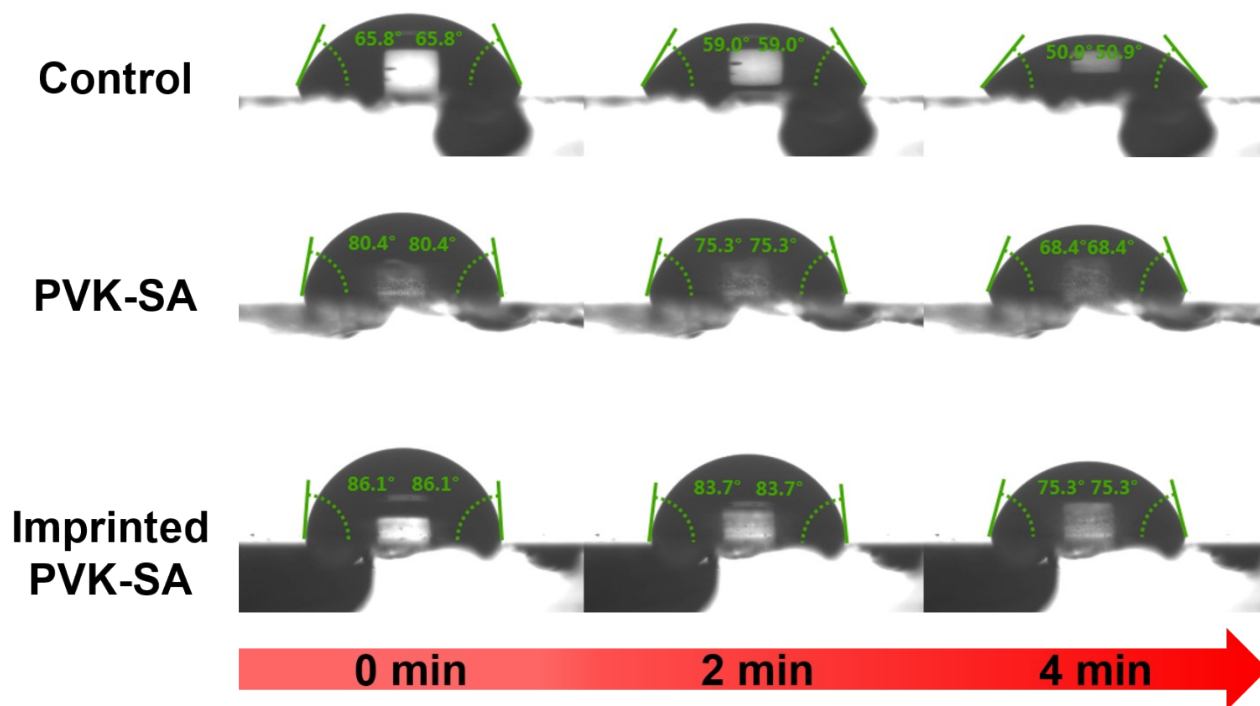
189



190

191 **Figure S22.** Vertical dark J - V curve of ITO/FAMAPbI₃/Ag.

192

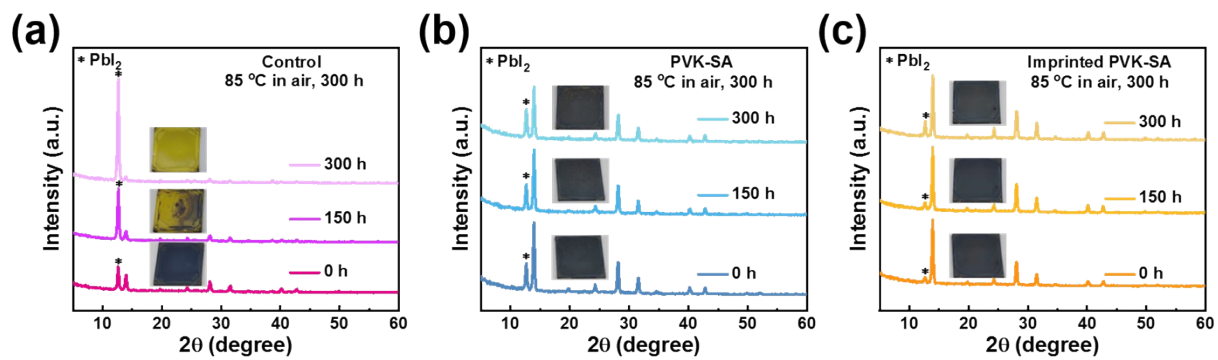


193

194 **Figure S23.** The dynamic contact angles on the surfaces of control, PVK-SA and imprinted PVK-SA

195 perovskite films, respectively.

196



197

198 **Figure S24.** XRD patterns of control, PVK-SA and imprinted PVK-SA perovskite films deposited on

199 ITO/SnO₂ substrate heated at 85 °C in air for 300 h.

200

201 **Table S1.** The Brunauer-Emmett-Teller (BET) surface area and total pore volume for various PbI_2
202 films.

Sample	Surface area ($\text{m}^2 \text{g}^{-1}$)	Single point surface area ($\text{m}^2 \text{g}^{-1}$)	Total pore volume (cc g^{-1})
PbI_2	30.33	22.61	0.025
$\text{PbI}_2\text{-SA}$	39.03	27.64	0.034
Imprinted $\text{PbI}_2\text{-SA}$	84.94	73.65	0.076

203

204 **Table S2.** The parameters of time-resolved photoluminescence measurement of control, PVK-SA
205 and imprinted PVK-SA perovskite films, respectively.

Sample	τ_1 (ns)	τ_2 (ns)	A	B₁ (%)	B₂ (%)	τ_{ave} (ns)
Control	41.2	715.8	6.6	2.74	97.26	494
PVK-SA	53.5	1463.1	71.1	0.86	99.14	1194
Imprinted PVK-SA	89.2	1979.1	119.7	0.27	99.73	1870

206

207 **Table S3.** A list of recently reported perovskite solar cells with high efficiency that fabricated with
 208 two-step sequential deposition method.

Perovskite type	V_{oc} (V)	PCE (%)	Ref
$FA_{1-x}MA_xPbI_3$	1.16	23.56	[1]
$FA_{1-x}MA_xPbI_3$	1.148	22.35	[2]
$BA_xFA_yMA_zPbI_3$	1.18	23.15	[3]
$FA_{1-x}MA_xPbBr_yI_{3-y}$	1.152	21.87	[4]
$FA_xCs_yMA_zPbI_3$	1.06	21.5	[5]
FAPbI ₃	1.116	22.04	[6]
FAPbI ₃	1.182	25.6	[7]
$FA_{1-x}MA_xPbI_3$	1.18	24.37	[8]
$(FAPbI_3)_x(MAPbI_3)_y$	1.12	22.53	[9]
$FA_{1-x}MA_xPbI_3$	1.150	23.56	This work

209

210 **Table S4.** Space-limited charge current (SCLC) calculation results of the hole-only and electron-only
211 devices based on the control, PVK-SA and imprinted PVK-SA PVSCs, respectively.

Devices	Hole trap density (cm⁻³)	Electron trap density (cm⁻³)
Control	5.90×10 ¹⁵	4.24×10 ¹⁵
PVK-SA	3.13×10 ¹⁵	3.60×10 ¹⁵
Imprinted PVK-SA	1.10×10 ¹⁵	1.01×10 ¹⁵

213 **Table S5.** A list of recently reported 5 cm ×5 cm perovskite solar modules with high efficiency that
 214 fabricated with two-step sequential deposition method.

Perovskite type	V_{oc} (V)	J_{sc} [mA cm^{-2}]	FF [%]	PCE [%]	Ref
MAPbI ₃	5.26	3.70	66.11	12.86	[10]
FA _{1-x} MA _x PbI ₃	6.19	2.62	68.00	11.07	[11]
(FAPbI ₃) _{1-x} (MAPbBr ₃) _x	6.71	3.47	71.00	16.54	[12]
FAMAPbI ₃	7.31	2.96	67.23	14.55	[13]
FA_{1-x}MA_xPbI₃	5.33	4.51	68.37	16.42	This work

215

216 **References**

- 217 [1] Q. Jiang, Y. Zhao, X. Zhang, X. Yang, Y. Chen, Z. Chu, Q. Ye, X. Li, Z. Yin, J. B. You, *Nat. Photon.*
218 **2019**, 13, 460.
- 219 [2] Y. P. Zhao, P. C. Zhu, S. Huang, S. Tan, M. H. Wang, R. Wang, J. J. Xue, T. H. Han, S. J. Lee, A.
220 Zhang, T. Y. Huang, P. Cheng, D. Meng, J. W. Lee, J. Marian, J. Zhu, Y. Yang, *J. Am. Chem. Soc.*
221 **2020**, 142, 20071
- 222 [3] H. K. Zhang, M. C. Qin, Z. L. Chen, W. Yu, Z. W. Ren, K. Liu, J. M. Huang, Y. K. Zhang, Q. Liang, H.
223 T. Chandran, P. W. K. Fong, Z. J. Zheng, X. H. Lu, G. Li, *Adv. Mater.* **2021**, 33, 2100009.
- 224 [4] Z.C. Lin, W. Q. Zhang, Q. B. Cai, X. N. Xu, H. Y. Dong, C. Mu, J. P. Zhang, *Adv. Sci.* **2021**, 8, 2102845.
- 225 [5] C. H. Chen, Y. H. Lou, K. L. Wang, Z. H. Su, C. Dong, J. Chen, Y. R. Shi, X. Y. Gao, Z. K. Wang, *Adv.*
226 *Energy Mater.* **2021**, 11, 2101538.
- 227 [6] J. He, H. L. Liu, F. Zhang, X. G. Li, S. R. Wang, *Adv. Funct. Mater.* **2022**, 32, 2110030
- 228 [7] Y. Zhao, F. Ma, Z. H. Qu, S. Q. Yu, T. Shen, H. X. Deng, X. B. Chu, X. X. Peng, Y. B. Yuan, X. W.
229 Zhang, J. B. You, *Science* **2022**, 377, 531.
- 230 [8] T. Zhou, Z. Y. Xu, R. Wang, X. Y. Dong, Q. Fu, Y. S. Liu, *Adv. Mater.* **2022**, 2200705.
- 231 [9] X. B. Zhang, W. C. Zhou, X. Q. Chen, Y. C. Chen, X. H. Li, M. Q. Wang, Y. Zhou, H. Yan, Z. L. Zheng,
232 Y. Z. Zhang, *Adv. Energy Mater.* **2022**, 2201105.
- 233 [10] F. Matteocci, L. Vesce, F. U. Kosasih, L. A. Castriotta, S. Cacovich, A. L. Palma, G. Divitini, C.
234 Ducati, A. D. Carlo, *ACS Appl. Mater. Interfaces* **2019**, 11, 25195.
- 235 [11] Z. Q. Huang, X. T. Hu, Z. Xing, X. C. Meng, X. P. Duan, J. Long, T. Hu, L. C. Tan, Y.W. Chen, *J. Phys.*
236 *Chem. C* **2020**, 124, 8129.
- 237 [12] J. W. Zhang, T. L. Bu, J. Li, H. Y. Li, Y. P. Mo, Z. L. Wu, Y. F. Liu, X. L. Zhang, Y. B. Cheng, F. Z.
238 Huang, *J. Mater. Chem. A* **2020**, 8, 8447.
- 239 [13] G. Q. Tong, D. Son, L. K. Ono, Y. Q. Liu, Y. Q. Hu, H. Zhang, A. Jamshaid, L. B. Qiu, Z. H. Liu, Y. B.
240 Qi, *Adv. Energy Mater.* **2021**, 11, 2003712.